Computational and Theoretical Chemistry 1234 (2024) 114531

Contents lists available at ScienceDirect

Computational and Theoretical Chemistry

journal homepage: www.elsevier.com/locate/comptc

Alkali metal decorated BC_3 monolayer as sensing material for warfare agents

Sajida Munsif [a], Khurshid Ayub [b], Mohammad Nur-e-Alam [c], Dmitry Nerukh [d], Zaheer Ul-Haq [a,*]

[a] Dr. Panjwani Center for Molecular Medicine and Drug Research, ICCBS, University of Karachi, Karachi 75270, Pakistan
[b] Department of Chemistry, COMSATS University Islamabad, Abbottabad Campus, KPK, 22060, Pakistan
[c] Department of Pharmacognosy, College of Pharmacy, King Saud University, P.O. Box. 2457, Riyadh 11451, Kingdom of Saudi Arabia
[d] Department of Mathematics, Aston University, Birmingham, United Kingdom

A B S T R A C T

This study investigates the adsorption properties and electronic characteristics of pristine and alkali metal (Li, Na, K)-decorated BC_3 monolayers for the detection of toxic warfare agents, crucial for environmental protection and human health. Physisorption is observed for H_2CO, $COCl_2$, and $CSCl_2$ on the BC_3 monolayer, with adsorption energies of −8.06, −8.63, and −9.56 kcal/mol, respectively. Alkali metal decoration induces chemisorption, significantly enhancing adsorption energies (e.g., H_2CO on KBC_3 with −20.85 kcal/mol). $LiBC_3$ and KBC_3 exhibit high sensitivity to $CSCl_2$ and $COCl_2$, respectively, with short recovery times (4.59 and 2.72 *sec*). The reduced work function (ϕ) (4.34) of $CSCl_2$@$LiBC_3$ compared to pristine BC_3 (4.98) confirms the heightened sensitivity of $LiBC_3$ to $CSCl_2$. Therefore, Li and K-decorated BC_3 monolayers emerge as promising candidates for $CSCl_2$ and $COCl_2$ sensors, offering strong adsorption, high sensitivity, and rapid recovery times.

1. Introduction

Graphene is made up of a single layer of carbon atoms that are arranged in a two-dimensional honeycomb lattice [1,2]. It has a high surface area, excellent mechanical stability, and excellent thermal conductivity [3]. It can be used in a variety of applications, including optical devices [4], energy generation and storage [5,6], and chemical sensors [7]. Graphene is a viable option for use as a gas sensor because it exhibits extremely conducive properties even at zero carrier density [8]. The charge-carrier concentration between the graphene sheet and the adsorbed gas molecules typically changes, which can be used to detect sensitive sensors [9]. Moreover, many experimental and theoretical studies have shown that adding impurities and defects can change the physical characteristics and chemical sensitivity of graphene sheets [10–13], indicating a significant potential of decorated graphene for use in gas-sensing and catalysis devices. Inspired by the astonishing gas sensing performance of graphene, the sensing capability of other 2D structures such as MoS_2 [14–16], WS_2 [17,18], phosphorene [19,20], boron nitride [21–23], silicene [24], graphene-like BC_3 monolayer [25,26], germanene [27,28], $PtTe_2$ monolayer [29], ZnS monolayer [30], monolayer Janus MoSSe [31],C_3N monolayer [32], NiS_2 monolayer [33], PdS_2 monolayer [34] toward various gases has also been investigated.

Additionally, studies have shown that the BC_3 monolayer is a semiconductor compared to graphene which is a semimetal with a band gap of zero [35–38]. A two-dimensional honeycomb-like structure having a stoichiometry of BC_3 has been experimentally fabricated [39–41]. The honeycomb lattice of BC_3 sheet is nearly identical to that of graphene, with the exception that some carbon atoms are swapped out for boron atoms, forming a hexagon with six carbon atoms surrounded by six boron atoms. Recently, the BC_3 monolayer has been recognized for its exceptional stability, good mechanical properties, optical characteristics, and electronic and thermal transport properties [42–44]. It is considered one of the most potential candidates in various fields such as catalysis, batteries, gas sensing, nano-electronics, and energy storage materials [37,38,45–49]. It has been demonstrated that a BC_3 nanosheet is a monolayer film that exhibits exceptional crystalline quality (with mechanical strength comparable to graphene) [39]. The majority of the BC_3 structure is made up of boron–carbon and carbon–carbon bonds [35,40,41,50].

Numerous studies have shown that the electrical properties, surface reactivity, and sensing behavior of BC_3 nanosheets can be altered by the introduction of defects [51,52] and metal (or non-metal) dopants [26,53,54]. Many studies in the literature reported the interactions of various gas molecules (H_2, H_2O, H_2S, and NH_3) with perfect [25,45], imperfect [55], metal decorated [26,38], and BC_3 substrates. In addition, the BC_3 sheet with Li, Sc, and Fe adatom is an ideal material for a useful H_2 storage medium [56–58]. Moreover, silicon and aluminum

* Corresponding author.
E-mail address: zaheer.qasmi@iccs.edu (Z. Ul-Haq).

https://doi.org/10.1016/j.comptc.2024.114531
Received 9 September 2023; Received in revised form 31 December 2023; Accepted 26 February 2024
Available online 28 February 2024

doped BC_3 monolayer is highly sensitive to formaldehyde molecules [38]. Zhao *et al.* investigated the adsorption behaviors and optical properties of CH_3COCH_3, HCOH, HCN, H_2O, SO_2, CO_2, H_2, N_2, and O_2 molecules on the BC_3 monolayer and depicted that BC_3 monolayer as a room-temperature acetone gas sensor is highly sensitive and selective towards these gas molecules and has rapid response and recovery time [25].

Metal-doped BC_3 monolayer is highly sensitive to carbonyl pollutants [38]. These carbonyl compounds are environmental pollutants that cause severe effects on humans such as headache, asthma, eye, and nose, and throat irritation. As a result, even a small amount of these poisonous compounds can have serious negative impacts on the environment and the general public [59]. Moreover, the increase of these toxic chemicals in the environment is gaining the attention of the World Health Organization for public health. These chemicals cause severe complications to human health and are also used in various activities [60]. Phosgene ($COCl_2$), used as a chemical weapon during World War I, is a colorless, highly reactive, and extensively produced industrial lethal gas with a suffocating smell. It is used in many industries as a valuable organic raw material for the production of pharmaceuticals, polycarbonates, polymers, pesticides, dyes, and isocyanates [61]. Prolonged exposure to $COCl_2$ causes serious complications for all living organisms. For instance, it can cause distal lung damage, latent non-cardiogenic pulmonary edema, and irritation of the mucosal membrane, and at high concentrations, it is life-threatening [62]. Similarly, thiophosgene ($CSCl_2$) is a toxic gas with a strong suffocating smell. Besides, it has been used in the manufacture of various compounds and it is also employed as a chemical weapon. It causes severe lung damage, mainly causes irritation to sensitive body parts, and often leads to death [63]. Whereas, formaldehyde (HCHO), a volatile noxious gas and an important organic pollutant, is widely used industrially for the manufacture of different materials including polymers, plywood, building boards, and lacquer materials [64–66]. It causes significant eye and skin inflammation in addition to seriously harming the neurological, respiratory, and endocrine systems [66]. Above a particular threshold, its higher concentration causes severe cancerous illnesses [65]. Since these substances ultimately result in cancer under extreme circumstances, it is crucial to find them to monitor and control the situation [65]. Accordingly, establishing economical, quick, innovative, and futuristic techniques or special materials for examining and regulating the disclosure of these dangerous compounds is a crucial challenge for sensor technology. However, a number of studies are reported in literature regarding the sensing of these toxic gases. The density functional theory studies employed to determine the adsorption behavior and electronic properties of phosgene and formaldehyde on pristine and metal-doped phthalocyanine monolayers suggested that the pristine phthalocyanine monolayer is not suitable for phosgene and formaldehyde sensing due to its weak adsorption strength. However, the Al-doped phthalocyanine monolayer is a promising material for toxic phosgene and formaldehyde gas detection because of its strong ability to adsorb these two gases [67]. Sattar *et al.* investigated the selectivity and sensitivity of twisted nanographene analogs towards phosgene, thiophosgene, and formaldehyde and found that all the selected toxic chemicals are physisorbed on the surfaces of twisted nanographene. Moreover, the electronic parameters support the highest selectivity and sensitivity of twisted nanographene towards thiophosgene compared to formaldehyde and phosgene [68].

Besides all these studies, the alkali metal doped BC_3 monolayer has still not been investigated for the sensing of phosgene, thiophosgene, and formaldehyde gases. The rational of considering lightweight alkali metals for decoration is their cohesive energies as compared to heavy elements like transitions metals which have high cohesive energies. This would enable uniform distributions of lightweight alkali metals over BC_3 monolayer without forming clusters as the metal bindings surpass the corresponding metal cohesive energies. When heavy elements are doped, cohesive energies tend to be higher than the corresponding binding energies. This leads to the development of clusters and subsequently compromises the reversibility of the doped systems. Moreover, functionalization of graphene-like BC_3 with alkali (Li, Na, K) is a useful strategy to improve the sensitivity of monolayer [49]. Therefore, here we are interested in investigating the potential possibility of pristine and alkali metal-doped BC_3 monolayer for the sensing of phosgene, thiophosgene, and formaldehyde.

2. Computational methodology

Geometry optimizations, energy calculations, and density of states (DOS) analysis have been performed on BC_3 monolayer and its complexes with phosgene, thiophosgene, and formaldehyde using ωB97XD functional with 6–31G (d,p) basis set as implemented in Gaussian 16 suite of program. A geometric optimization without any constraints is performed for the free gaseous molecules (analytes), pristine and alkali metal doped BC_3 monolayer, gas/monolayer complex.

The convergence criteria for each geometry optimization was:

Maximum Force 3.8×10^{-5}.
RMS Force 5.0×10^{-5}.
Maximum Displacement 9.2×10^{-4}.
RMS Displacement 1.3×10^{-4}.

Vibrational frequency analysis was also performed which confirmed the optimized geometries as true minima with all positive frequencies. GaussView 5.0 and Chemcraft software are used for structural analysis and visualization of optimized geometries. GaussSum program has been used to obtain the DOS results. We have defined adsorption energy in the usual way:

The adsorption energy (E_{ad}) of phosgene, thiophosgene, and formaldehyde (indexed here by X) with isolated BC_3 and M-BC_3 was calculated.

$$E_{ad} = E_{X-BC3} - (E_X + E_{BC3}) \quad (1)$$

where $E_{X\text{-}BC3}$, E_X, and E_{BC3} are the energies of gas/pure and doped monolayer, free gas molecules, and pure BC_3 monolayer, respectively.

The chemical potential (μ), hardness (η), softness (s), and electrophilicity index (ω) are calculated by using the following formula: [69,70]

$$\mu \approx (E_{HOMO} + E_{LUMO}) \quad (2)$$

$$\eta \approx \frac{1}{2}(\mathrm{ELUMO} - \mathrm{EHOMO}) \quad (3)$$

$$\omega \approx \frac{\mu^2}{2\eta} \quad (4)$$

3. Results and discussion

3.1. Optimized geometries of pristine and alkali metal decorated BC_3 monolayer

The adsorption behavior of formaldehyde, phosgene, and thiophosgene is analyzed on pristine and alkali metal decorated BC_3 monolayer. For this purpose, the geometries of all three analytes and BC_3 monolayer are optimized using ωB97XD functional with 6-31G (d,p) basis set. It has 21B atoms and 68C atoms. Here the end atoms are saturated with 25H atoms to avoid the boundary effects. The geometry of the optimized BC_3 monolayer has two types of bonds, namely C—C and B–C, with corresponding bond lengths of 1.41 and 1.57 Å, respectively, as depicted in Fig. 1(a) and are in good agreement with the previous literature [25,49]. There are two different types of hollow sites in BC_3 nanosheet (as shown in Fig. 1(a)), one is the hollow center of the C_6 hexagon whereas the other one is the C_4B_2 hexagon.

The optimized geometries of BC_3 monolayer decorated with alkali

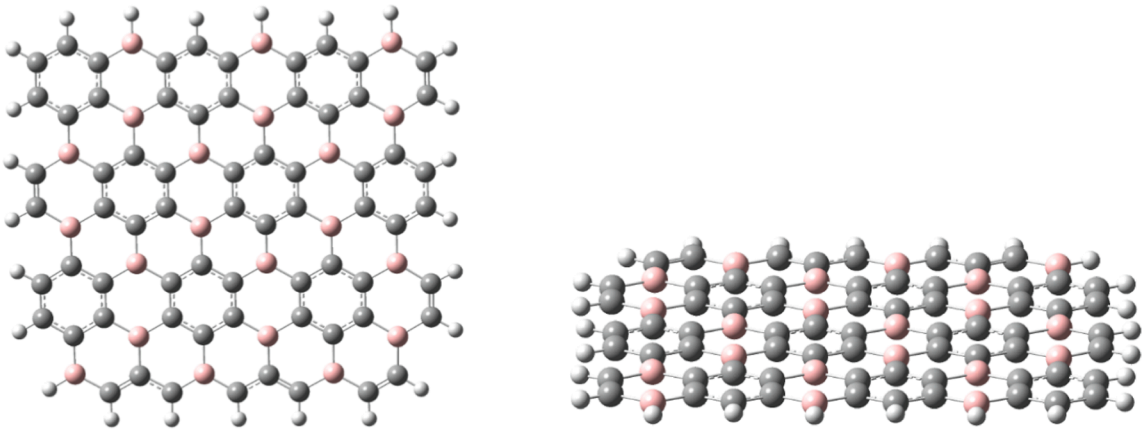

Fig. 1a. Optimized geometry of pristine BC_3 monolayer top and side view.

metals (Li, Na, and K) are shown in Fig. 1(b). The alkali metal atoms bind on the hollow site of BC_3 hexagon where the binding distances of BC_3 with Li, Na, and K are 1.90, 2.34, and 2.95 Å respectively, (Fig. 1b), which is also in good agreement with the literature [49]. The adsorption energy of Li@BC_3 is −56.67 kcal/mol indicative of strong interaction of Li with BC_3 monolayer. Similarly, Na also interacted strongly with the monolayer resulting in an interaction complex having adsorption energy of −48.72 kcal/mol. Moreover, the E_{ads} of K is the highest (−59.38 kcal/mol) among all the three alkali metal atoms indicating a much higher stability of the K-doped BC_3 among all.

3.2. Adsorption of formaldehyde, phosgene, and thiophosgene on pristine BC_3 monolayer

After optimization of BC_3 monolayer, the adsorption of formaldehyde, phosgene, and thiophosgene is scrutinized on a pristine monolayer. Initially, each analyte was adsorbed at the surface of a pristine BC_3 monolayer in different orientations (vertically and horizontally) but after optimization, only one stable geometry was obtained for each analyte. It was observed that formaldehyde favored adsorbing at the top of the bond shared between boron and carbon atoms. However, it preferred to adsorb vertically via its oxygen atom interacting with boron while the hydrogen atom with the carbon of the monolayer, where, the interaction distance between B-O and C—H are 2.45 and 2.66 Å, respectively. Unlike formaldehyde, phosgene and thiophosgene adsorbed in parallel fashion on top of the bond shared between two carbon atoms of the BC_3 monolayer with an interaction distance of 3.52 and 3.50 Å, respectively. The top view and side view of the optimized geometries of analytes adsorbed on the surface of BC_3 monolayer are depicted in Fig. 2. The corresponding adsorption energies of the complexes H_2CO@BC_3, $COCl_2$@BC_3, and $CSCl_2$@BC_3 are −8.06, −8.63, and −9.56 kcal/mol, respectively. The interaction between analytes (formaldehyde, phosgene, and thiophosgene) and pristine BC_3 monolayer can be regarded as physical adsorption thus suggesting the poor capture capability of BC_3 monolayer towards these analytes.

3.3. Adsorption of H_2CO, $COCl_2$, and $CSCl_2$ on alkali metal (Li, Na, K) decorated BC_3 monolayer

Adsorption of formaldehyde, phosgene, and thiophosgene is also

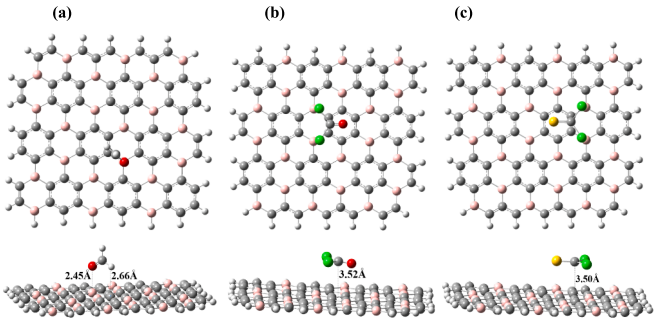

Fig. 2. Top view and side view of the optimized geometries of (a) H_2CO@BC_3, (b) $COCl_2$@BC_3, (c) $CSCl_2$@BC_3 monolayer.

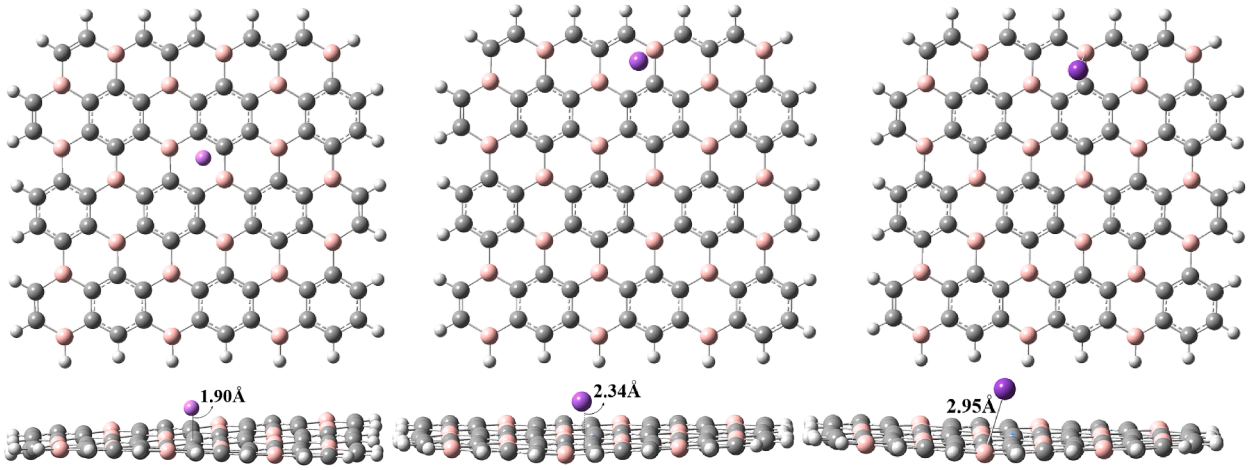

Fig. 1b. Optimized geometries of alkali metal (a) Li, (b) Na, (c) K) decorated BC_3 monolayer.

investigated on alkali metal doped BC_3 monolayer to check the effect of alkali metal decoration on the sensing performance of BC_3 monolayer. For this purpose, geometries are optimized with analytes adsorbed at the surface of the alkali metal decorated BC_3 monolayer. It is observed that the interaction distance of Li-sheet after the adsorption of analytes changed, Li-sheet distance increased to 1.95 Å after the adsorption of formaldehyde from 1.90 Å (before the adsorption of formaldehyde). Likewise, the interaction distance of Li and BC_3 monolayer is increased to 1.99 Å after the adsorption of thiophosgene. However, the interaction distance between Li and BC_3 monolayer decreased to 1.84 Å after adsorption of phosgene.

The optimized geometries of H_2CO@$LiBC_3$, $COCl_2$@$LiBC_3$, and $CSCl_2$@$LiBC_3$ are presented in Fig. 3. During optimization, H_2CO adsorb at the surface in such a way that its O atom got closer to the Li atom resulting in an interaction distance of about 1.89 Å. The corresponding adsorption energy of H_2CO@$LiBC_3$ was −42.89 kcal/mol. The small bond length of Li-O and more negative E_{ads} indicate that the doping of Li on BC_3 monolayer can improve the reactivity of BC_3 towards formaldehyde molecule. The H_2CO binds with the Li atom, which is electron-deficient and can receive electrons from the lone pair orbital of oxygen.

Consequently, phosgene and thiophosgene are adsorbed at the surface of $LiBC_3$ in a parallel fashion in such a way that their chlorine atoms interact with the Li atom. The interaction distance between Cl and Li atoms is 2.81 (2.84) and 2.71 Å, respectively. Whereas, the corresponding adsorption energies are −25.62 and −17.29 kcal/mol. The adsorption energy value calculated here for Li decorated BC_3 monolayer for phosgene adsorption is weak chemisorption comparable to already reported values [71,72]. These results indicated that the adsorption of formaldehyde, phosgene, and thiophosgene on Li-decorated BC_3 monolayer is weak chemisorption.

Additionally, based on adsorption energy values, BC_3 monolayer decorated with Na is a promising sensing material that exhibits significantly greater sensitivity towards formaldehyde than the previously reported system [63]. The adsorption energies of H_2CO@$NaBC_3$, $COCl_2$@$NaBC_3$, and $CSCl_2$@$NaBC_3$ are −22.82, −11.98, and −14.40 kcal/mol, respectively and the corresponding geometries are depicted in Fig. 4. The adsorption energy of formaldehyde on Na decorated BC_3 monolayer is more effective than thiophosgene. It is observed that the interaction distance of Na from BC_3 monolayer increased to 2.38 Å upon adsorption of formaldehyde, but decreased to 2.32 and 2.33 Å after adsorption of phosgene and thiophosgene respectively, form 2.34 Å (before adsorption of formaldehyde). The interaction distance of Na from the oxygen atom of formaldehyde is 2.26 Å. Moreover, formaldehyde preferred to adsorb at the surface of $NaBC_3$ with an interaction distance of 3.10 Å from the sheet. In addition, all the analytes adsorbed at the surface of the Na decorated monolayer in a parallel fashion.

Consequently, the adsorption of all three analytes on potassium decorated BC_3 monolayer resulted in an increase in the interaction distance of K from the sheet, where the distance increased from 2.95 Å (before adsorption of analytes) to 3.05, 2.98, and 3.04 Å for formaldehyde, phosgene, and thiophosgene, respectively. Moreover, formaldehyde and phosgene interacted with K via their oxygen atom with an interaction distance of 2.60 and 2.66 Å, respectively. However, the interaction distance of carbon of formaldehyde and phosgene from the sheet are 3.00 and 3.37 Å, respectively. Thiophosgene on the other hand interacted with K via its chlorine, carbon, and sulphur atoms. The interaction distances are shown in Fig. 5. The adsorption energies of the respective complexes are −20.85, 16.98, and −14.99 kcal/mol, respectively. The results of adsorption energy values suggested that potassium-decorated BC_3 monolayer is a promising material for phosgene sensing as compared to formaldehyde and thiophosgene.

3.4. Dipole moment and NBO charge transfer analysis

The change in the dipole moments of pristine and decorated BC_3 monolayer is analyzed before and after the adsorption of analytes and the corresponding dipole moment values are listed in Table 1. The value of the dipole moment depends on the magnitude and the separation of the columbic charges between interacting species. A higher value of dipole moment indicates higher charge transfer from one molecule to another in a complex. The dipole moment of the pristine BC_3 monolayer is 2.96 D. However, the dipole moments are increased upon the adsorption of the alkali metals. For instance, the dipole moments of $LiBC_3$, $NaBC_3$, and KBC_3 are increased to 10.08, 7.02, and 9.13 respectively. Thus the dopant elements enhanced the dipole moment of BC_3. Additionally, upon the adsorption of the toxic analytes (H_2CO, $COCl_2$, and $CSCl_2$) on the surface of BC_3 monolayer, the dipole moments are increased to 4.39, 3.06, and 2.98 D respectively, compared to pristine BC_3 monolayer (2.96). The highest dipole moment is observed for H_2CO@BC_3, which is due to the large charge separation between hydrogen atoms of formaldehyde and the π-electronic cloud of BC_3 monolayer. However, the decrease in the value of dipole moment for $COCl_2$@BC_3 may be due to the less charge separation between interacting chlorine atom and π-electrons of BC_3 monolayer, (Cl-π-C). Similarly, the dipole moment is further reduced for $CSCl_2$@BC_3 to 2.98 D, because the magnitude of charges is reduced due to the replacement of oxygen (in phosgene) with less electronegative sulfur atom in thiophosgene. In addition, the dipole moments of all the analytes adsorbed

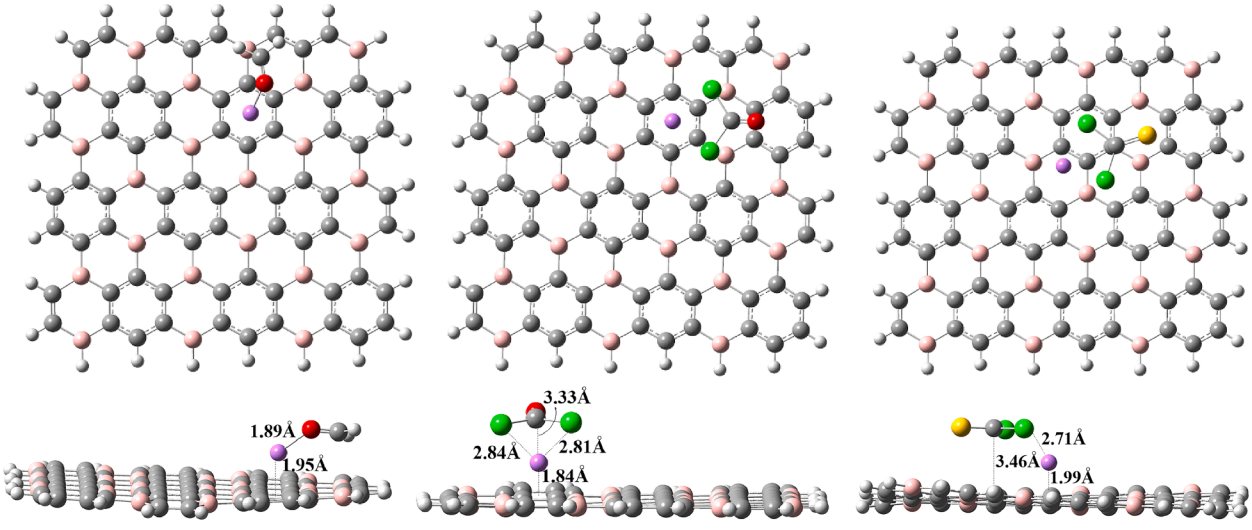

Fig. 3. Optimized geometries of H_2CO@$LiBC_3$, $COCl_2$@$LiBC_3$, $CSCl_2$@$LiBC_3$ top view, (left) and side view (right).

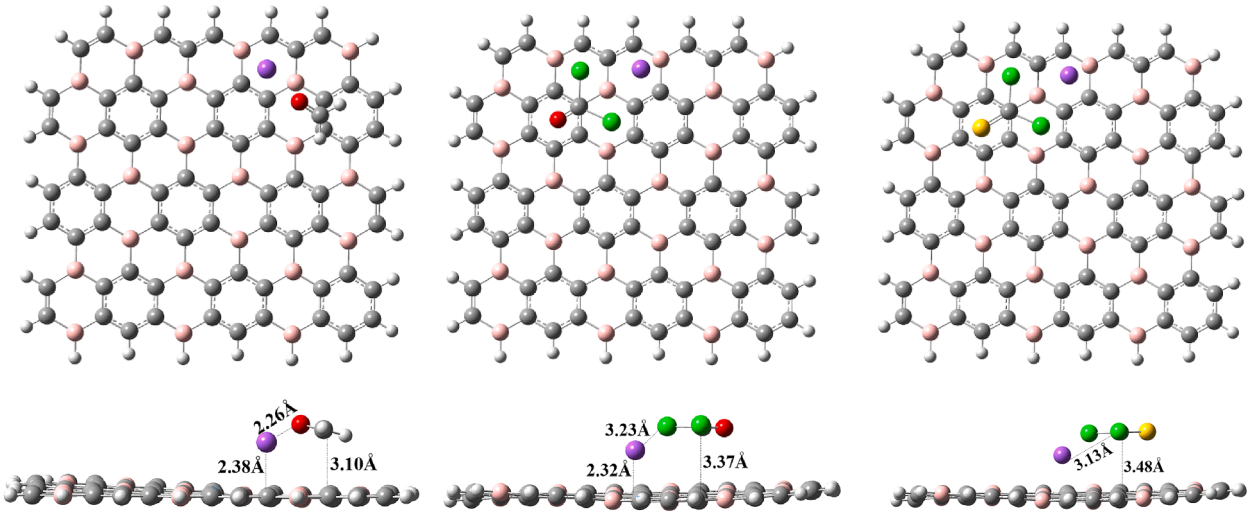

Fig. 4. Optimized geometries of $H_2CO@NaBC_3$, $COCl_2@NaBC_3$, $CSCl_2@NaBC_3$ top view, (left) and side view (right).

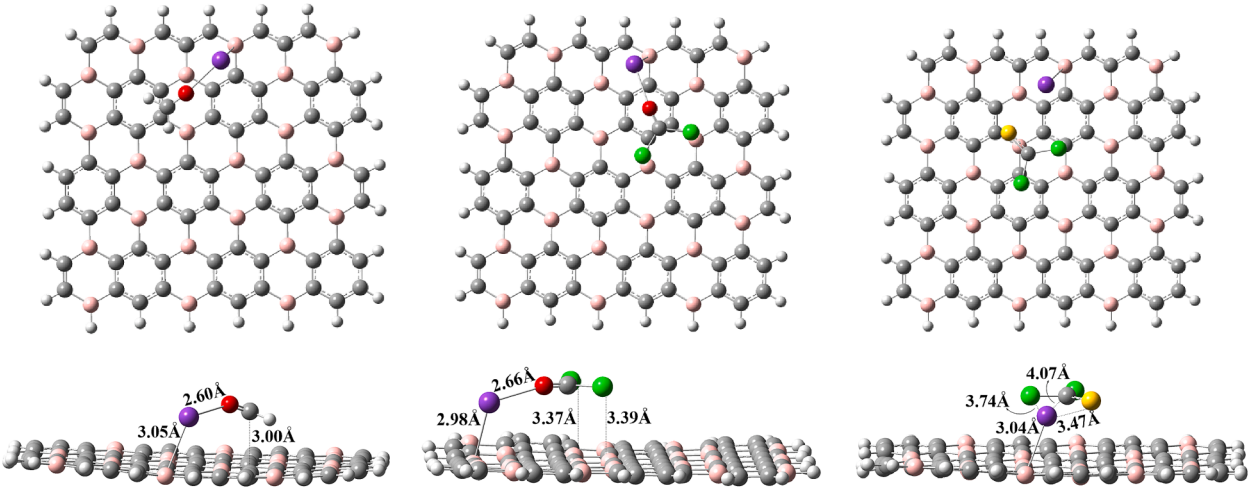

Fig. 5. Optimized geometries of $H_2CO@KBC_3$, $COCl_2@KBC_3$, $CSCl_2@KBC_3$ top view, (left) and side view (right).

Table 1
Adsorption energies (E_{ads}, kcal/mol), Dipole moments (μ, debye), charge (Q, e), and the recovery time (τ, *sec*) of formaldehyde, phosgene, and thiophosgene on pristine and alkali metal decorated BC_3 monolayer.

System	E_{ads}	μ	Q	τ
BC_3		2.97		
$LiBC_3$	−56.67	10.08	0.424	
$NaBC_3$	−48.72	7.02	0.526	
KBC_3	−59.38	9.13	0.754	
$H_2CO@BC_3$	−8.06	4.39	0.089	
$COCl_2@BC_3$	−8.63	3.06	0.018	
$CSCl_2@BC_3$	−9.56	2.98	0.020	
$H_2CO@LiBC_3$	−42.89	4.00	−0.058	2.57×10^{19}
$COCl_2@LiBC_3$	−25.62	6.17	0.059	5.80×10^{6}
$CSCl_2@LiBC_3$	−17.29	9.52	0.051	4.59
$H_2CO@NaBC_3$	−22.82	7.55	0.005	5.15×10^{4}
$COCl_2@NaBC_3$	−11.98	6.85	0.035	5.94×10^{-4}
$CSCl_2@NaBC_3$	−14.40	6.51	0.024	0.035
$H_2CO@KBC_3$	−20.85	7.99	−0.003	1.86×10^{3}
$COCl_2@KBC_3$	−16.98	8.91	0.031	2.72
$CSCl_2@KBC_3$	−14.99	8.39	0.028	0.095

at the surface of alkali metal (Li, Na, K) decorated BC_3 monolayer further increased (Table 1) to several orders of magnitude compared to the pristine BC_3 monolayer. Thus, the increase of dipole moments after the adsorption of analytes indicates that significant amounts of charges are transferred and it also indicates that an attractive interaction exists between the adsorbate and adsorbent in a complex.

The charge transfer analysis plays an important role in the detailed evaluation of the electronic behavior and interaction mechanism between BC_3 monolayer and the toxic analytes. The NBO charge transfer analysis has been performed to demonstrate the extent of charge transfer between BC_3 monolayer (pristine and alkali metal decorated) and the toxic analytes during complexation. All the computed NBO charges are given in Table 1. An investigation into the charge transfer between analytes and BC_3 monolayer indicates that the charges are transferred from analytes to BC_3 monolayer. $H_2CO@BC_3$, $COCl_2@BC_3$, and $CSCl_2@BC_3$ had charge transfers of 0.089, 0.018, and 0.020 e, respectively. However, alkali metal (Li, Na, K) decorated BC_3 had respective charge transfer amounts of 0.424, 0.526, and 0.754 e, respectively. Table 1 lists the charge transfer of each analyte at alkali metal decorated BC_3 complexes.

3.5. Frontier molecular orbital (FMO) analysis

The interaction between molecules takes place due to the overlapping of the FMO [73]. Thus, FMO analysis is performed to measure the changes in the electronic densities of the pristine and alkali metal

decorated BC_3 monolayer upon interaction with selected toxic analytes. The orbital analysis determines the conductivity while investigating the highest occupied molecular orbital (HOMO) and lowest unoccupied molecular orbital (LUMO) energy gap (E_g). The E_g is obtained from the following relation:

$$E_g = E_L - E_H \tag{5}$$

In addition to investigate the sensing ability of BC_3 monolayer for these toxic pollutants, the electronic properties of the optimized geometries are evaluated. The electronic properties provide significant information for the sensitivity, conductivity, resistivity, and selectivity of BC_3 monolayer towards these toxic molecules [45,74,75]. For instance, the decrease in HOMO–LUMO gaps (EH-L) reflects the increase in electrical conductivity, higher electronic distribution, and greater sensitivity whereas the resistivity increases with an increase in the HOMO–LUMO gap of a system [68,76–78].

The HOMO LUMO gap of pristine BC_3 monolayer was 4.56 eV. However, it was observed that the HOMO LUMO gap of Na and K decorated BC_3 monolayer is increased (4.93, 4.84 eV, respectively) while that of $LiBC_3$ is decreased (3.93 eV) from 4.56 eV (pristine BC_3 monolayer). Moreover, the HOMO LUMO gap remains unchanged after the adsorption of analytes on pristine monolayer which suggests that the analytes adsorption has no influence on the resistivity of pristine BC_3 monolayer and thus has poor sensitivity towards these analytes. In addition, the energy gap of the $LiBC_3$ monolayer increased to 4.67, 4.53, and 4.05 eV after the adsorption of H_2CO, $COCl_2$, and $CSCl_2$ gas molecules from 3.93 ($LiBC_3$). Moreover, E_g of $H_2CO@NaBC_3$, $COCl_2@NaBC_3$, and $CSCl_2@NaBC_3$ reduced to 4.85, 4.91, and 4.86 eV respectively, from 4.93 eV (E_g of $NaBC_3$). Similarly, the reduction in E_g is observed for $H_2CO@KBC_3$, $COCl_2@KBC_3$, and $CSCl_2@KBC_3$ (4.71, 4.78, 4.70 eV, respectively) compared to KBC_3 monolayer (4.84 eV). Consequently, the FMO analysis suggested that the interaction of toxic chemicals with decorated BC_3 monolayer produced a more pronounced effect on the HOMO energies, which is responsible for a decrease in the HOMO LUMO energy gap.

Further, the isosurfaces of HOMO and LUMO of $H_2CO@BC_3$, $COCl_2@BC_3$, and $CSCl_2@BC_3$ are presented in Fig. 6, which shows that densities of HOMO and LUMO orbitals are delocalized on the surface of the BC_3. However, these HOMO densities are localized on BC_3 monolayer, upon interaction with toxic analytes, the HOMO densities are shifted towards the analyte as in the case of formaldehyde adsorption on $LiBC_3$. The variation in HOMO and LUMO densities and their HOMO LUMO energy gaps (E_g) upon interaction with analytes significantly affect the conductivity of a semiconducting material [79]. Furthermore, the isosurfaces of HOMO and LUMO of analytes at alkali metal decorated (Li, Na, K) are presented in Figs. 7, 8, and 9, respectively.

The electrical conductivity (EC) increases with a decrease in the HOMO LUMO energy gap of semiconducting material [63]. The EC can be determined by equation (6).[63]

$$\mathrm{EC} = AT^{\frac{3}{2}}e^{\frac{-E_g}{2kT}} \tag{6}$$

where k is the Boltzmann's constant (8.617×10^{-5} eV K^{-1}) and T is the temperature in K (298 K). Conductivity is exponentially associated with the E_g, so it increases with the reduction in E_g. For further investigation of the sensitivity of the alkali metal decorated BC_3 monolayer towards toxic analytes, the E_{FL} and work function (ϕ) of all the complexes are studied and summarized in Tables 2, and 3. ϕ is defined as the energy required to remove an electron from the Fermi level to a vacuum level at an infinite distance away outside the surface. ϕ can be calculated by the following equation:

$$\acute{E}_{,} = \mathrm{Vel}(+\infty) - \mathrm{EF} \tag{7}$$

where E_F denotes the Fermi level energy and $V_{el(+\infty)}$ is the electron electrostatic potential energy far from the surface of the material which has been supposed to be zero. Thus the work function is the negative of Fermi energy. The change of ϕ of the alkali metal decorated BC_3 monolayer upon toxic analyte adsorption alters the field emission properties of the monolayer. The results depicted in Table 3 show that the ϕ of $H_2CO@LiBC_3$, $COCl_2@LiBC_3$, and $CSCl_2@LiBC_3$ are reduced to 4.37, 4.65, and 4.34 respectively, from 4.98 (pristine BC_3, Table 2), confirming the high sensitivity of $LiBC_3$ towards the thiophosgene gas molecule as compared to formaldehyde and phosgene. Similarly, the work function of $H_2CO@NaBC_3$ is reduced to 4.33 from 4.35 ($NaBC_3$) whereas, that of $COCl_2@NaBC_3$ increased to 4.36 and the work function of $CSCl_2@NaBC_3$ remained the same i.e., 4.35 (Table 3) compared to $NaBC_3$. Similarly, the work function of $H_2CO@KBC_3$ and $CSCl_2@KBC_3$ remained the same (see Table 3) compared to KBC_3 (Table 2), however, the work function value of $COCl_2@KBC_3$ is reduced compared to KBC_3 confirming the sensitivity of KBC_3 monolayer towards phosgene. These results suggested that alkali metal doping is an encouraging way of increasing the sensitivity of BC_3 towards these toxic gases which was not possible using the pristine BC_3.

Finally, the effective desorption of a gas molecule (adsorbate) from the adsorbent surface is also of great significance in assessing the repeatability of the gas sensor. A good gas sensor must have a quick recovery time for its sustainable utilization. Based on the transition state theory, recovery time (τ) is related to adsorption energy and it can be calculated by using the following equation [80]

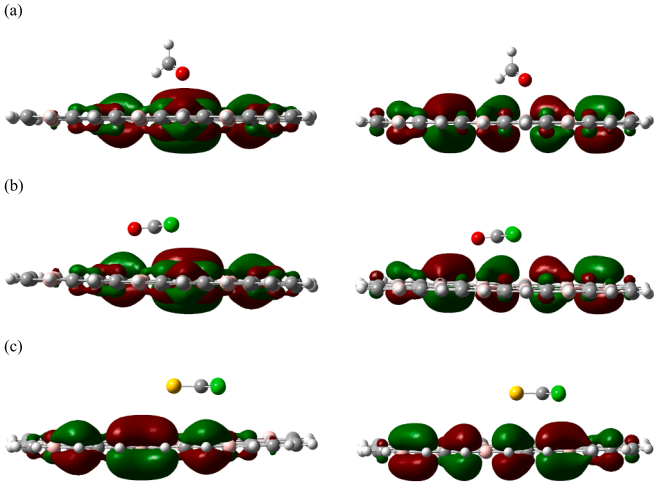

Fig. 6. HOMO (left) and LUMO (right) of (a) $H_2CO@BC_3$, (b) $COCl_2@BC_3$, (c) $CSCl_2@BC_3$.

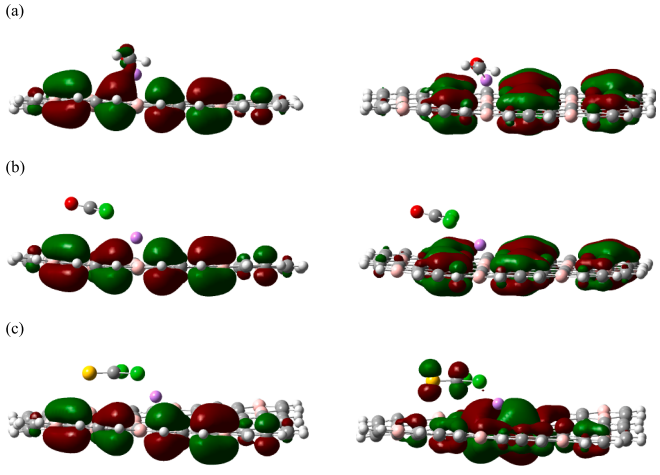

Fig. 7. HOMO (left) and LUMO (right) representation of (a) $H_2CO@LiBC_3$, (b) $COCl_2@LiBC_3$, (c) $CSCl_2@LiBC_3$.

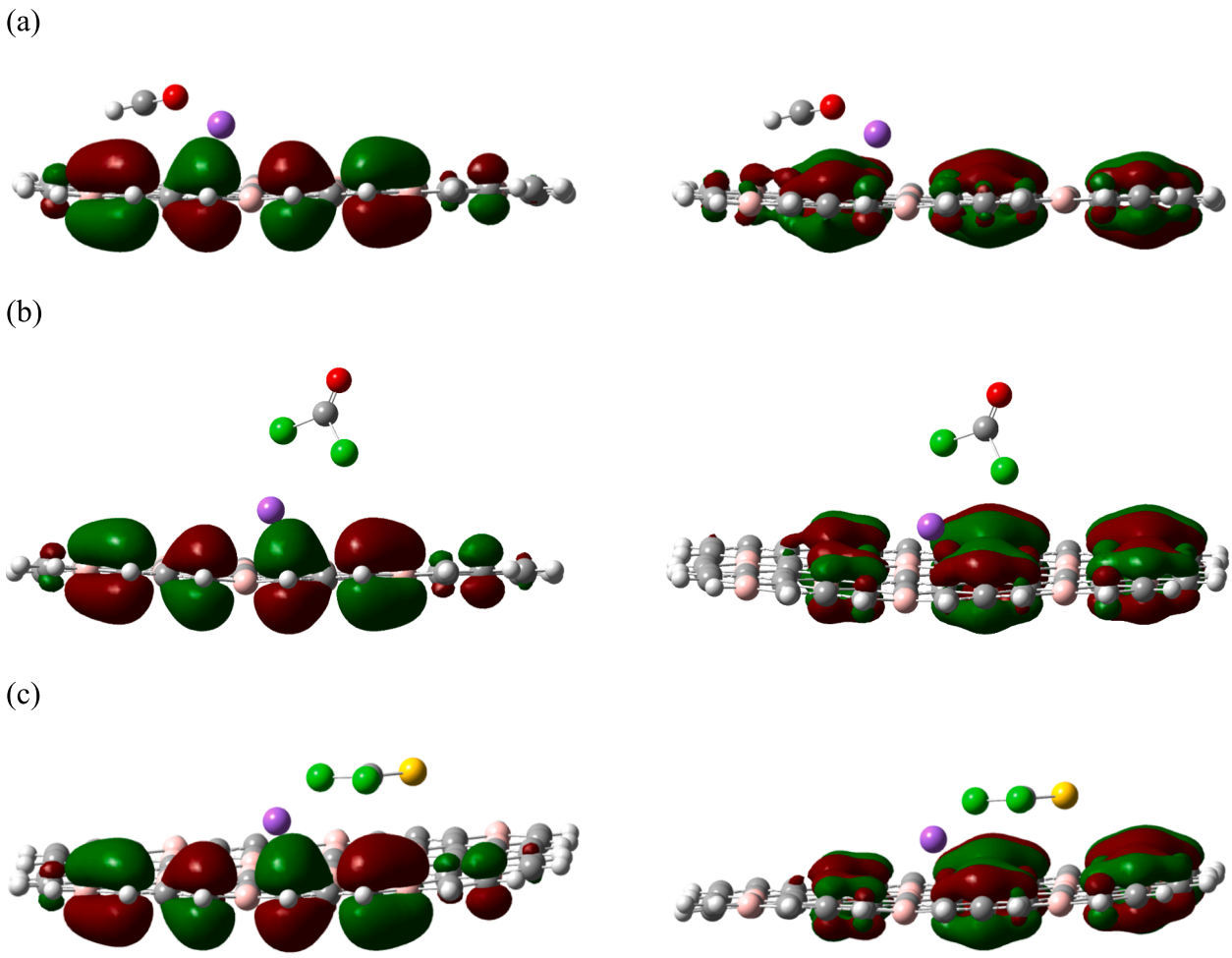

Fig. 8. HOMO (left) and LUMO (right) representation of (a) $H_2CO@NaBC_3$, (b) $COCl_2@NaBC_3$, (c) $CSCl_2@NaBC_3$.

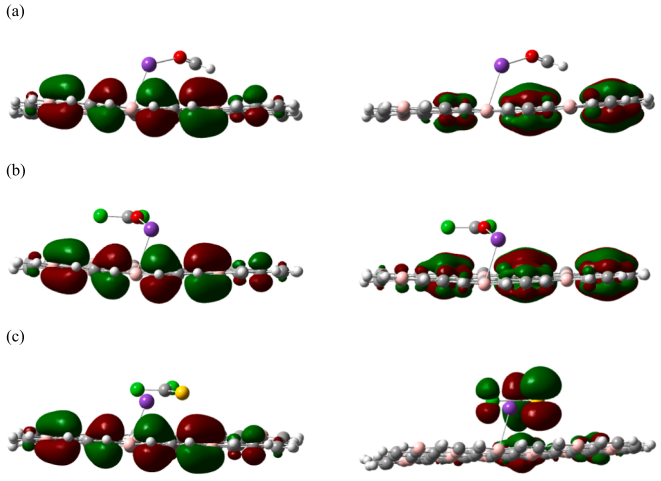

Fig. 9. HOMO (left) and LUMO (right) representation of (a) $H_2CO@KBC_3$, (b) $COCl_2@KBC_3$, (c) $CSCl_2@KBC_3$.

$$\tau = \upsilon_0^{-1} exp\left(\frac{-E_{ads}}{KT}\right) \quad (8)$$

where υ_0 represents the attempt frequency, T is the temperature, and K is the Boltzmann constant (1.99×10^{-3} kcal/mol K). In the present work, the value of attempt frequency is taken as 1×10^{-12} s^{-1}, according to reported literature [81,82]. The calculated recovery time (Table 1) of formaldehyde at room temperature (298 K) is higher for $LiBC_3$, $NaBC_3$, and KBC_3 which suggested that these alkali metal decorated monolayers are appropriate as adsorbents for the removal of formaldehyde instead as a reusable sensor because of their long recovery time and a strong ability to adsorb the gas. Likewise, the recovery time of phosgene for $LiBC_3$ is also higher, thus not a suitable reusable sensor for phosgene. However, the recovery time of phosgene for $NaBC_3$, and KBC_3 are 5.94 $\times 10^{-14}$ and 2.72 *sec*. On the other hand, the recovery time of thiophosgene for $LiBC_3$, $NaBC_3$, and KBC_3 is short i.e., 4.59, 0.035, and 0.095 *sec* respectively, therefore, the alkali metal decorated BC_3 monolayer could be suitable as reusable sensors for the detection of thiophosgene at room temperature due to their high sensitivity and short recovery time.

3.6. Global reactivity parameters

The adsorption effect of formaldehyde, phosgene, and thiophosgene on pure and alkali metal decorated BC_3 monolayer is also scrutinized from global reactivity parameters. The chemical potential (μ), chemical hardness (η), softness (s), and electrophilicity index (ω) are calculated and shown in Tables 2, and 3, respectively, for all the systems. These global reactivity descriptors predict the stability and reactivity of the studied complexes. Electrophilicity is related to the chemical reactivity of a compound. The pure BC_3 monolayer has an electrophilicity value of 5.44 eV. The electrophilicity values decreased upon the adsorption of analytes on pure and alkali metal decorated BC_3 monolayer which suggests that all the systems are less reactive compared to pristine BC_3 monolayer. Similarly, the value of chemical potential (μ) has a direct

Table 2
Energies of HOMO (E_H), LUMO (E_L) orbitals, and HOMO-LUMO energy gap (E_g), energy of Fermi level ($\mathbf{E_{FL}}$), work function ($\boldsymbol{\phi}$), chemical potential (μ), chemical hardness (η), softness (s) and electrophilicity (ω) of pristine BC_3, alkali metal decorated BC_3 and analytes@BC_3 in eV.

Systems	E_H	E_L	E_g	E_{FL}	ϕ	μ	η	s	ω
BC_3	−7.26	−2.70	4.56	−4.98	4.98	4.98	2.28	0.22	5.44
$LiBC_3$	−6.36	−2.43	3.93	−4.39	4.39	4.39	1.96	0.26	4.92
$NaBC_3$	−6.82	−1.89	4.93	−4.35	4.35	4.35	2.46	0.2	3.85
KBC_3	−6.70	−1.86	4.84	−4.28	4.28	4.28	2.42	0.21	3.78
$H_2CO@BC_3$	−7.25	−2.69	4.56	−4.97	4.97	4.97	2.28	0.22	5.42
$COCl_2@BC_3$	−7.27	−2.70	4.57	−4.99	4.99	4.98	2.28	0.22	5.44
$CSCl_2@BC_3$	−7.26	−2.70	4.56	−4.98	4.98	4.98	2.28	0.22	5.44

Table 3
Energies of HOMO (E_H), LUMO (E_L) orbitals, and HOMO-LUMO energy gap (E_g), energy of Fermi level ($\mathbf{E_{FL}}$), work function ($\boldsymbol{\phi}$), chemical potential (μ), chemical hardness (η), softness (s) and electrophilicity (ω) of analytes@$LiBC_3$, analytes@$NaBC_3$, and analytes@KBC_3 in eV.

Systems	E_H	E_L	E_g	E_{FL}	ϕ	μ	η	s	ω
$H_2CO@LiBC_3$	−6.71	−2.04	4.67	−4.37	4.37	4.37	2.33	0.21	4.10
$COCl_2@LiBC_3$	−6.60	−2.07	4.53	−4.65	4.65	4.65	2.26	0.22	4.80
$CSCl_2@LiBC_3$	−6.37	−2.32	4.05	−4.34	4.34	4.34	2.03	0.25	4.64
$H_2CO@NaBC_3$	−6.75	−1.90	4.85	−4.33	4.33	4.33	2.43	0.21	3.86
$COCl_2@NaBC_3$	−6.81	−1.90	4.91	−4.36	4.36	4.36	2.46	0.20	3.86
$CSCl_2@NaBC_3$	−6.78	−1.92	4.86	−4.35	4.35	4.35	2.43	0.21	3.89
$H_2CO@KBC_3$	−6.63	−1.92	4.71	−4.28	4.28	4.27	2.35	0.21	3.88
$COCl_2@KBC_3$	−6.64	−1.86	4.78	−4.25	4.25	4.25	2.39	0.21	3.78
$CSCl_2@KBC_3$	−6.63	−1.93	4.70	−4.28	4.28	4.28	2.35	0.21	3.90

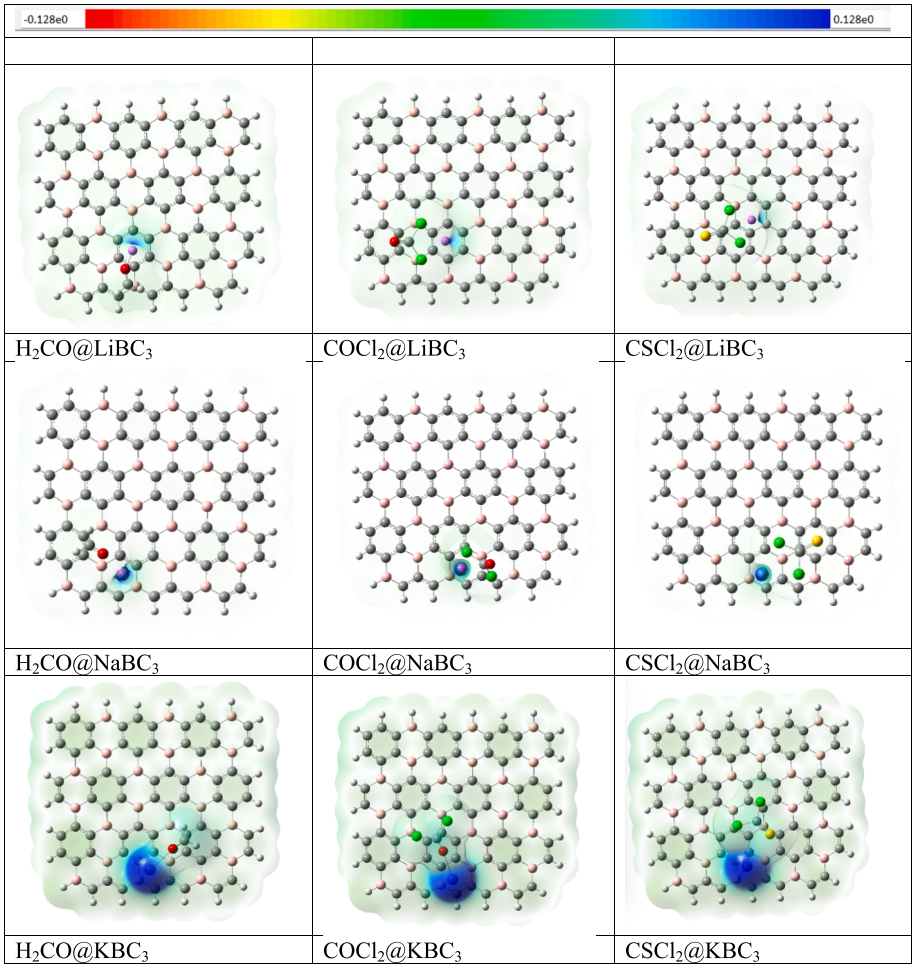

Fig. 10. Electrostatic potential maps of adsorbed H_2CO, $COCl_2$, and $CSCl_2$ gas molecules on alkali metal decorated BC_3 monolayer.

relation with the chemical stability and an inverse relation with the reactivity of the system. The higher values of chemical potential indicate that all the complexes are thermodynamically stable and less reactive. Moreover, the chemical hardness and softness of a compound are directly related to its chemical stability (low reactivity). It is observed that the value of chemical hardness increased for all the systems compared to pristine BC_3 monolayer, confirming the stability of the complexes. All our systems are hard in nature with a low value of global softness. Additionally, the chemical hardness provides information about the characteristics of a surface to resist electronic charge within its environment [22]. A higher value of chemical hardness and E_H implies higher stability and lower reactivity whereas, a low value of chemical hardness and E_H suggests less stability and higher reactivity of the systems. Our results indicate that analytes at Li-decorated BC_3 monolayer are more stable and are less reactive compared to $LiBC_3$ monolayer (Table 3). However, the interaction of analytes with Na and K decorated BC_3 monolayer causes an appreciable decrease in η and E_H values as compared to $NaBC_3$ and KBC_3 monolayer which shows less stability and high reactivity of the complexes (Table 3). However, as compared to pristine BC_3 monolayer all the systems are more stable and less reactive.

3.7. Molecular electrostatic potential

The molecular electrostatic potential calculations are used to analyze electron density distribution over the molecule. It provides information for predicting the reactivity of the molecule towards nucleophilic and electrophilic attacks [83]. It also gives information about the intermolecular interactions, simultaneously demonstrating the positive, negative and neutral electrostatic potential regions, as well as molecular size and shape [84]. The red color portion represents the negative potential region with higher electron density, while the blue region is electropositive, indicating lower electron density. In Fig. 10, electrostatic potential maps of adsorbed H_2CO, $COCl_2$, and $CSCl_2$ gas molecules on alkali metal decorated BC_3 monolayer are presented. The figure depicts that the positive electrostatic potential is concentrated near the decorated alkali metal atom and adjacent carbon atoms, making it a favorable site for nucleophilic attack. The green color representats zero electrophilicity, indicating a nonreactive site, as shown in Fig. 10.

4. Conclusions

We investigated the adsorption of toxic warfare agents, including H_2CO, $COCl_2$, and $CSCl_2$ molecules, by DFT using pristine and alkali metal (Li, Na, K) decorated BC_3 monolayers, aiming to seek a novel gas sensing material for the detection or removal of warfare agents. Our results show that the pristine BC_3 monolayer has less potential to be used as a gas-sensing material for these warfare agents due to their poor adsorption strength. However, the decoration of BC_3 monolayer with alkali metals enhanced the interactions between BC_3 and adsorbed toxic gas molecules. The adsorption of these harmful gases on alkali metal decorated BC_3 monolayers resulted in chemisorption. The adsorption energy of H_2CO, $COCl_2$, and $CSCl_2$ on $LiBC_3$ is −42.89, −25.62, and −17.29 kcal/mol, respectively, whereas on $NaBC_3$, it is −22.82, −11.98, and −14.40 kcal/mol, respectively. However, the adsorption energy of the analytes on KBC_3 is improved to −20.85, −16.98, and −14.99 kcal/mol, respectively. Based on FMO analysis, the $LiBC_3$ monolayer exhibits a high sensitivity towards $CSCl_2$ molecule due to a decrease in E_g and variation of electrical conductivity. The highest decrease in the HOMO LUMO gap (4.05 eV) is observed for $CSCl_2$@$LiBC_3$ which suggests its higher conductivity compared to all other systems. Additionally, a quick response to desorption was observed for the $CSCl_2$@$LiBC_3$ and $COCl_2$@KBC_3, with recovery times of 4.59 and 2.72 *sec*, respectively, at room temperature. Overall, the alkali metal decorated BC_3 monolayer is one of the potential candidates for phosgene and thiophosgene sensors, as it shows good stability, adsorption strength, high sensitivity, and fast recovery time.

CRediT authorship contribution statement

Sajida Munsif: Formal analysis, Methodology. **Khurshid Ayub:** Investigation, Validation, Visualization, Writing – original draft. **Mohammad Nur-e-Alam:** Funding acquisition, Writing – review & editing. **Dmitry Nerukh:** Software, Writing – review & editing. **Zaheer Ul-Haq:** .

Declaration of competing interest

The authors declare that they have no known competing financial interests or personal relationships that could have appeared to influence the work reported in this paper.

Data availability

Data will be made available on request.

Acknowledgments

The authors extend their appreciation to the Researchers Supporting Project number (RSPD2024R994), King Saud University, Riyadh, Saudi Arabia

References

[1] K.S. Novoselov, A.K. Geim, The rise of graphene, Nat. Mater. 6 (2007) 1–14.
[2] A.K. Geim, Graphene: status and prospects, Science 324 (2009) 1530–1534.
[3] R.S. Edwards, K.S. Coleman, Graphene synthesis: relationship to applications, Nanoscale 5 (2013) 38–51.
[4] J. Kang, J. Li, F. Wu, S.S. Li, J.B. Xia, Elastic, electronic, and optical properties of two-dimensional graphyne sheet, J. Phys. Chem. C 115 (2011) 20466–20470.
[5] M. Pumera, Graphene-based nanomaterials for energy storage, Energy Environ. Sci. 4 (2011) 668–674.
[6] Z. Xiang, Q. Dai, J.-F. Chen, L. Dai, Edge functionalization of graphene and two-dimensional covalent organic polymers for energy conversion and storage, Adv. Mater. 28 (2016) 6253–6261.
[7] F. Yavari, N. Koratkar, Graphene-based chemical sensors, J. Phys. Chem. Lett. 3 (2012) 1746–1753.
[8] O. Leenaerts, B. Partoens, F.M. Peeters, Adsorption of H_2O, NH_3, CO, NO_2, and NO on graphene: a first-principles study, Phys. Rev. B - Condens. Matter. Mater. Phys. 77 (12) (2008) 125416.
[9] F. Schedin, A. K. Geim, S. V. Morozov, E. W. Hill, P. Blake, M. I. Katsnelson, K. S. Novoselov, Detection of individual gas molecules adsorbed on graphene, Nat. Mater. 6 (9) (2007) 652–655.
[10] Y.H. Zhang, Y.B. Chen, K.G. Zhou, C.H. Liu, J. Zeng, H.L. Zhang, Y. Peng, Improving gas sensing properties of graphene by introducing dopants and defects: a first-principles study, Nanotechnology 20 (18) (2009) 185504–185511.
[11] J. Dai, J. Yuan, P. Giannozzi, Gas adsorption on graphene doped with B, N, Al, and S: a theoretical study, Appl. Phys. Lett. 95 (23) (2009) 232105.
[12] T. Hussain, P. Panigrahi, R. Ahuja, Sensing propensity of a defected graphane sheet towards CO, H_2O and NO_2, Nanotechnology. 25 (32) (2014) 325501–325506.
[13] Q. Zhou, W. Ju, X. Su, Y. Yong, X. Li, Adsorption behavior of SO_2 on vacancy-defected graphene: a DFT study, J. Phys. Chem. Solids 109 (2017) 40–45.
[14] H. Wei, Y. Gui, J. Kang, W. Wang, C. Tang, A DFT study on the adsorption of H_2S and SO_2 on Ni doped MoS_2 monolayer, Nanomaterials 8 (2018) 1–12.
[15] D. Ma, W. Ju, T. Li, X. Zhang, C. He, B. Ma, Z. Lu, Z. Yang, The adsorption of CO and NO on the MoS_2 monolayer doped with Au, Pt, Pd, or Ni: A first-principles study, Appl. Surf. Sci. 383 (2016) 98–105.
[16] J. Zhu, H. Zhang, Y. Tong, L. Zhao, Y. Zhang, Y. Qiu, X. Lin, First-principles investigations of metal (V, Nb, Ta)-doped monolayer MoS2: Structural stability, electronic properties and adsorption of gas molecules, Appl. Surf. Sci. 419 (2017) 522–530.
[17] M. O'Brien, K. Lee, R. Morrish, N.C. Berner, N. McEvoy, C.A. Wolden, G. S. Duesberg, Plasma assisted synthesis of WS_2 for gas sensing applications, Chem. Phys. Lett. 615 (2014) 6–10.
[18] N. Huo, S. Yang, Z. Wei, S.S. Li, J.B. Xia, J. Li, Photoresponsive and gas sensing field-effect transistors based on multilayer WS_2 nanoflakes, Sci. Rep. 4 (2014) 1–9.
[19] S. Guo, L. Yuan, X. Liu, W. Zhou, X. Song, S. Zhang, First-principles study of SO_2 sensors based on phosphorene and its isoelectronic counterparts: GeS, GeSe, SnS, SnSe, Chem. Phys. Lett. 686 (2017) 83–87.
[20] R. Bhuvaneswari, R. Chandiramouli, First-principles investigation on detection of phosgene gas molecules using phosphorene nanosheet device, Chem. Phys. Lett. 717 (2019) 99–106.
[21] F. Behmagham, E. Vessally, B. Massoumi, A. Hosseinian, L. Edjlali, A computational study on the SO_2 adsorption by the pristine, Al, and Si doped BN nanosheets, Superlatt. Microstruct. 100 (2016) 350–357.

[22] M.D. Mohammadi, H.Y. Abdullah, H. Louis, G.E. Mathias, 2D boron nitride material as a sensor for H_2SiCl_2, Comput. Theor. Chem. 1213 (2022) 113742.
[23] A.A. Peyghan, M. Noei, S. Yourdkhani, Al-doped graphene-like BN nanosheet as a sensor for para-nitrophenol: DFT study, Superlatt. Microstruct. 59 (2013) 115–122.
[24] R. Chandiramouli, A. Srivastava, V. Nagarajan, NO adsorption studies on silicene nanosheet: DFT investigation, Appl. Surf. Sci. 351 (2015) 662–672.
[25] Z. Zhao, Y. Yong, R. Gao, S. Hu, Q. Zhou, X. Su, Y. Kuang, X. Li, Adsorption, sensing and optical properties of molecules on BC3 monolayer: First-principles calculations, Mater. Sci. Eng. B Solid-State Mater. Adv. Technol. 271 (6) (2021): 115266.
[26] M. M. Kadhim, A. M. Rheima, Z. S. Sabri, B. Al-Qargholi, A. S. Jaber, F. M. D. Al-Jaafari, W. Al-Azzawi, S. K. Hachim,D. T. Zaidan, T. Z. Taban, A density functional study on the sensing behavior of copper doped BC_3 nanosheet toward COS gas, Inorg. Chem. Commun. 152 (4) (2023) 110689.
[27] V. Nagarajan, R. Chandiramouli, NO_2 adsorption behaviour on germanene nanosheet – a first-principles investigation, Superlatt. Microstruct. 101 (2017) 160–171.
[28] S. M. Aghaei, M. M. Monshi, I. Torres, I. Calizo. Efficient and Reversible CO_2 Capture by Lithium-functionalized Germanene Monolayer, arvix.org (2017) 1–5.
[29] Z. Xu, Adsorption and sensing mechanisms of Ni-doped $PtTe_2$ monolayer upon NO_2 and O_3 in air-insulated switchgears, RSC Adv. 13 (2023) 18129–18137.
[30] L. Chhana, B. Lalroliana, R.C. Tiwari, B. Chettri, L. Pachuau, S. Gurung, L. Vanchhawng, D.P. Rai, L. Zuala, R. Madaka, Theoretical study of ZnS monolayer adsorption behavior for CO and HF gas molecules, ACS Omega 7 (44) (2022) 40176–40183.
[31] H. Chen, J. Pang, J. Zhang, G. Wei, S. Wei, J. Yan, Exploring monolayer Janus MoSSe as potential gas sensor for Cl2, H2S and SO2, Comput. Theor. Chem. 1211 (2022) 113665.
[32] H. Cui, C. Yan, P. Jia, W. Cao, Adsorption and sensing behaviors of SF6 decomposed species on Ni-doped C3N monolayer: a first-principles study, Appl. Surf. Sci. 512 (2020) 145759.
[33] H. Wu, Y. Xia, C. Zhang, S. Xie, S. Wu, H. Cui, Adsorptions of C5F10O decomposed compounds on the Cu-decorated NiS_2 monolayer: a first-principles theory, Mol. Phys. 121 (2023) e2163715.
[34] S. Zhai, X. Jiang, D. Wu, L. Chen, Y. Su, H. Cui, Single Rh atom decorated pristine and S-defected PdS2 monolayer for sensing thermal runaway gases in a lithium-ion battery: a first-principles study, Surf. Interf. 37 (2023) 102735.
[35] D. Tomanek, R.M. Wentzcovitch, S.G. Louie, M.L. Cohen, Calculation of electronic and structural properties of BC_3, Phys. Rev. B 37 (1988) 3134–3136, https://doi.org/10.1103/PhysRevB.37.3134.
[36] Y. Ding, Y. Wang, J. Ni, Electronic structures of BC_3 nanoribbons, Appl. Phys. Lett. 94 (2009) 1–4.
[37] A. Bafekry, S.S. Farjami, M. Ghergherehchi, F.M. Peeters, Tuning the bandgap and introducing magnetism into monolayer BC_3 by strain/defect engineering and adatom/molecule adsorption, J. Appl. Phys. 126 (2019).
[38] J. Beheshtian, A.A. Peyghan, M. Noei, Sensing behavior of Al and Si doped BC_3 graphenes to formaldehyde, Sens. Actuat. B Chem. 181 (2013) 829–834.
[39] H. Yanagisawa, T. Tanaka, Y. Ishida, M. Matsue, E. Rokuta, S. Otani, C. Oshima, Phonon dispersion curves of a BC_3 honeycomb epitaxial sheet, Phys. Rev. Lett. 93 (2004) 1–4.
[40] H. Tanaka, Y. Kawamata, H. Simizu, T. Fujita, H. Yanagisawa, S. Otani, C. Oshima, Novel macroscopic BC_3 honeycomb sheet, Solid State Commun. 136 (2005) 22–25.
[41] H. Yanagisawa, T. Tanaka, Y. Ishida, E. Rokuta, S. Otani, C. Oshima, Phonon dispersion curves of stable and metastable BC_3 honeycomb epitaxial sheets and their chemical bonding: experiment and theory, Phys. Rev. B - Condens. Matter. Mater. Phys. 73 (2006) 1–7.
[42] B. Mortazavi, M. Shahrokhi, M. Raeisi, X. Zhuang, L.F.C. Pereira, T. Rabczuk, Outstanding strength, optical characteristics and thermal conductivity of graphene-like BC_3 and BC_6N semiconductors, Carbon 149 (2019) 733–742.
[43] R.K. Zahedi, A.H.N. Shirazi, P. Alimouri, N. Alajlan, T. Rabczuk, Mechanical properties of graphene-like BC_3; a molecular dynamics study, Comput. Mater. Sci. 168 (2019) 1–10.
[44] J. Song, Z. Xu, X. He, Y. Bai, L. Miao, C. Cai, R. Wang, Thermal conductivity of two-dimensional BC3: a comparative study with two-dimensional C_3N, Phys. Chem. Chem. Phys. 21 (24) (2019) 12977–12985.
[45] S.M. Aghaei, M.M. Monshi, I. Torres, S.M.J. Zeidi, I. Calizo, DFT study of adsorption behavior of NO, CO, NO2, and NH3 molecules on graphene-like BC 3: a search for highly sensitive molecular sensor, Appl. Surf. Sci. 427 (2018) 326–333.
[46] Y. Qie, J. Liu, S. Wang, S. Gong, Q. Sun, C_3B monolayer as an anchoring material for lithium-sulfur batteries, Carbon 129 (2018) 38–44.
[47] Y. Tang, X. Cui, W. Chen, D. Zhu, H. Chai, X. Dai, A theoretical study on metal atom-modified BC_3 sheets for effects of gas molecule adsorptions, Appl. Phys. A Mater. Sci. Process. 124 (6) (2018).
[48] Y. Tang, M. Zhang, Z. Shen, J. Zhou, H. Chai, X. Dai, Non-metal atom anchored BC_3 sheet: A promising low-cost and high-activity catalyst for CO oxidation, New J. Chem. 42 (2018) 3770–3780.
[49] S.R. Naqvi, T. Hussain, S.R. Gollu, W. Luo, R. Ahuja, Superior sensitivity of metal functionalized boron carbide (BC3) monolayer towards carbonaceous pollutants, Appl. Surf. Sci. 512 (2020) 145637.
[50] Q. Wang, L.Q. Chen, J.F. Annett, Stability and charge transfer of B ordered structures, Phys. Rev. B - Condens. Matter. Mater. Phys. 54 (1996) R2271–R2275.
[51] Y. Ding, Y. Wang, J. Ni, Structural, electronic, and magnetic properties of defects in the BC_3 sheet from first principles, J. Phys. Chem. C 114 (2010) 12416–12421.
[52] S.S. Li, C.W. Zhang, W.X. Ji, F. Li, P.J. Wang, Tunable electronic properties induced by a defect-substrate in graphene/BC_3 heterobilayers, Phys. Chem. Chem. Phys. 16 (2014) 22861–22866.
[53] X. Lin, J. Ni, Electronic and magnetic properties of substitutionally Fe-, Co-, and Ni-doped BC_3 honeycomb structure, J. Appl. Phys. 111 (2012) 034309.
[54] M. Alizadeh, M.D. Esrafili, E. Vessally, Exploring surface reactivity of phosphorous-doped (6,0) and (4,4) BC3 nanotubes: A DFT study, J. Mol. Model. 19 (2013) 4877–4886.
[55] A.A. Peyghan, H. Soleymanabadi, S. Amir, Adsorption of H_2S at Stone-Wales defects of graphene-like BC_3: a computational study, Mol. Phys. 112 (2014) 2737–2745.
[56] T. Hussain, D.J. Searles, K. Takahashi, Reversible hydrogen uptake by BN and BC_3 monolayers functionalized with small Fe clusters: a route to effective energy storage, J. Phys. Chem. A 120 (2016) 2009–2013.
[57] S.R. Naqvi, T. Hussain, P. Panigrahi, W. Luo, R. Ahuja, Manipulating energy storage characteristics of ultrathin boron carbide monolayer under varied scandium doping, RSC Adv. 7 (2017) 8598–8605.
[58] Z. Yang, J. Ni, Li-doped BC_3 sheet for high-capacity hydrogen storage, Appl. Phys. Lett. 100 (2012) 2010–2014.
[59] H. Sajid, K. Ayub, T. Mahmood, Sensing behaviour of monocyclic C18 and B9N9 analogues toward chemical warfare agents (CWAs); quantum chemical approach, Surf. Interf. 30 (2022) 101912.
[60] H. John, M.J. van der Schans, M. Koller, H.E.T. Spruit, F. Worek, H. Thiermann, D. Noort, Fatal sarin poisoning in Syria 2013: forensic verification within an international laboratory network, Forensic Toxicol. 36 (2018) 61–71.
[61] P. Voßnacker, A. Wüst, T. Keilhack, C. Müller, S. Steinhauer, H. Beckers, S. Yogendra, Y. Schiesser, R. Weber, M. Reimann, R. Müller, M. Kaupp, S. Riedel, Novel synthetic pathway for the production of phosgene, Sci. Adv. 7 (40) (2021) 1–7.
[62] J. Pauluhn, Phosgene inhalation toxicity: Update on mechanisms and mechanism-based treatment strategies, Toxicology 450 (2021) 152682.
[63] O.D. Salahdin, H.H. Kzar, M.J.C. Opulencia, A.H. Abdulkadhim, A.T. Hammid, A. G. Ebadi, Potential application of AlP nanosheet semiconductor in the detection of toxic phosgene, thiophosgene, and formaldehyde gases, Semicond. Sci. Technol. 37 (9) (2022) 095015.
[64] Y.I. Korpan, M.V. Gonchar, A.A. Sibirny, C. Martelet, A.V. El'skaya, T.D. Gibson, A. P. Soldatkin, Development of highly selective and stable potentiometric sensors for formaldehyde determination, Biosens. Bioelectron. 15 (1–2) (2000) 77–83.
[65] L. Zhang, C. Steinmaus, D.A. Eastmond, X.K. Xin, M.T. Smith, Formaldehyde exposure and leukemia: a new meta-analysis and potential mechanisms, Mutat. Res. - Rev. Mutat. Res. 681 (2–3) (2009) 150–168.
[66] T. Salthammer, S. Mentese, R. Marutzky, Formaldehyde in the indoor environment, Chem. Rev. 110 (2010) 2536–2572.
[67] H. Xiong, B. Liu, H. Zhang, J. Qin, Theoretical insight into two-dimensional M-Pc monolayer as an excellent material for formaldehyde and phosgene sensing, Appl. Surf. Sci. 543 (2021) 148805.
[68] N. Sattar, H. Sajid, S. Tabassum, K. Ayub, T. Mahmood, M.A. Gilani, Potential sensing of toxic chemical warfare agents (CWAs) by twisted nanographenes: a first principle approach, Sci. Total. Environ. 824 (2022) 153858.
[69] R.G. Pearson, Absolute electronegativity and hardness correlated with molecular orbital theory, Proc. Natl. Acad. Sci. 83 (1986) 8440–8441.
[70] P.K. Chattaraj, U. Sarkar, D.R. Roy, Electrophilicity index, Chem. Rev. 106 (2006) 2065–2091.
[71] A.A. Menazea, N.S. Awwad, H.A. Ibrahium, K.H. Alharbi, M.S. Alqahtani, Titanium doping effect on the sensing performance of ZnO nanosheets toward phosgene gas, Phys. Scr. 97 (5) (2022) 055816.
[72] S. Hussain, R. Hussain, M.Y. Mehboob, S.A.S. Chatha, A.I. Hussain, A. Umar, M. U. Khan, M. Ahmed, M. Adnan, K. Ayub, Adsorption of phosgene gas on pristine and copper-decorated $B_{12}N_{12}$ nanocages: a comparative DFT study, ACS Omega 5 (2020) 7641–7650.
[73] S. Bibi, H. Ullah, S.M. Ahmad, A.U.H. Ali Shah, S. Bilal, A.A. Tahir, K., Ayub, Molecular and electronic structure elucidation of polypyrrole gas sensors, J. Phys. Chem. C 119 (28) (2015) 15994–16003.
[74] S. Khan, H. Sajid, K. Ayub, T. Mahmood, High sensitivity of graphdiyne nanoflake toward detection of phosgene, thiophosgene and phosogenoxime; a first-principles study, J. Mol. Graph. Model. 100 (2020) 107658.
[75] H. Louis, I.O. Amodu, T.O. Unimuke, T.E. Gber, B.B. Isang, A.S. Adeyinka, Modeling of Ca12O12, Mg12O12, and Al12N12 nanostructured materials as sensors for phosgene (Cl2CO), Mater. Today Commun. 32 (2022) 32:103946.
[76] H. Sajid, T. Mahmood, M.H.R. Mahmood, K. Ayub, Comparative investigation of sensor application of polypyrrole for gaseous analytes, J. Phys. Org. Chem. 32 (2019) 1–19.
[77] E. Balali, S. Sandi, M. Sheikhi, S. Shahab, S. Kaviani, DFT and TD-DFT study of adsorption behavior of Zejula drug on surface of the $B_{12}N_{12}$ nanocluster, Main Gr. Chem. 21 (2022) 405–420.
[78] S. Sarfaraz, M. Yar, M. Ans, M.A. Gilani, R. Ludwig, M.A. Hashmi, M. Hussain, S. Muhammad, Computational investigation of a covalent triazine framework (CTF-0) as an efficient electrochemical sensor, RSC. Adv. 12 (7) (2022) 3909–3923.
[79] H. Sajid, T. Mahmood, A DFT study on M3O (M = Li & Na) doped triphenylene and its amino-, hydroxy- and thiol-functionalized quantum dots for triggering remarkable nonlinear optical properties and ultra-deep transparency in ultraviolet region, Phys. E Low-Dimens. Syst. Nanostruct. 134 (2021).
[80] J. Zhang, L. Ma, M. Zhang, J. Zhang, Effects of gas adsorption on electronic and optical properties of palladium-doped graphene: first-principles study, Phys. E Low-Dimens. Syst. Nanostruct. 118 (2020) 113879.
[81] A. Sharma, theory Adsorption of phosgene on Si-embedded MoS2 sheet and electric field-assisted desorption : insights from DFT calculations, J. Mater. Sci. 54 (2019) 11497–11508.

[82] K. Patel, B. Roondhe, S.D. Dabhi, P.K. Jha, A new flatland buddy as toxic gas scavenger: a first principles study, J. Hazard. Mater. 351 (2018) 337–345.
[83] P. Sjoberg, P. Politzer, Use of the electrostatic potential at the molecular surface to interpret and predict nucleophilic processes, J. Phys. Chem. 94 (10) (1990) 3959–3961.
[84] P. Politzer, J.S. Murray, The fundamental nature and role of the electrostatic potential in atoms and molecules, Theor. Chem. Acc. 108 (3) (2002) 134–142.